Epidermal cell fusion promotes the transition from an embryonic to a larval transcriptome in *C. elegans*

Owen H. Funk, Daniel L. Levy*, David S. Fay*

Department of Molecular Biology, University of Wyoming, Laramie, WY 82071, USA

*Corresponding authors:

David S. Fay
University of Wyoming
Department of Molecular Biology
1000 E. University Avenue
Laramie, WY 82071
Phone: 307-766-4961
Fax: 307-766-5098
E-mail: davidfay@uwyo.edu

Daniel L. Levy
University of Wyoming
Department of Molecular Biology
1000 E. University Avenue
Laramie, WY 82071
Phone: 307-417-0354
Fax: 307-766-5098
E-mail: dlevy1@uwyo.edu

Abstract

Cell fusion is a fundamental process in the development of multicellular organisms, yet its impact on gene regulation, particularly during crucial developmental stages, remains poorly understood. The *Caenorhabditis elegans* epidermis comprises 8–10 syncytial cells, with the largest integrating 139 individual nuclei through cell–cell fusion governed by the fusogenic protein EFF-1. To explore the effects of cell fusion on developmental progression and associated gene expression changes, we conducted transcriptomic analyses of *eff-1* fusion-deficient mutants. Our RNAseq findings showed widespread transcriptomic changes that were enriched for epidermal genes and key molecular pathways involved in epidermal function during larval development. Subsequent single-molecule fluorescence *in situ* hybridization validated the altered expression of mRNA transcripts, confirming quantifiable changes in gene expression in the absence of embryonic epidermal fusion. These results underscore the significance of cell–cell fusion in shaping transcriptional programs during development and raise questions regarding the precise identities and specialized functions of different subclasses of nuclei within developing syncytial cells and tissues.

Introduction

Multinucleate syncytial cells are evolutionarily conserved and found throughout the tree of life in physiologically healthy tissue and disease states such as cancer (1-6). The need for a syncytium varies among organisms and tissues; multiple nuclei may be required to metabolically support larger cells or to facilitate the rapid production of large amounts of mRNA for developmental processes or in response to extracellular cues (7-11). There are multiple paths by which multinucleate syncytia arise, including cell–cell fusion of multiple mononucleate cells (1, 12-15). Cellular fusion necessarily merges the cytoplasm of two distinct cells, but how mixing of cytoplasmic factors changes the regulatory environment of individual nuclei within a newly formed syncytium is poorly understood (16-19).

The *C. elegans* epidermis (hypodermis) is an excellent model to address questions related to the function of syncytial nuclei; within this organism, which has a well-characterized and largely invariant cell lineage, over a third of somatic nuclei reside within

syncytial cells (14, 20). The worm epidermal system is a particularly tractable model and is composed (in the adult) of eight syncytial cells, the largest of which is hyp7, which surrounds most of the adult body (14). hyp7 forms through progressive rounds of cell fusion, beginning with 23 embryonic fusion events that create the initial larval hyp7 prior to hatching. This process is completely dependent on cell–cell fusion mediated by the fusogen EFF-1 followed by the addition of 116 additional nuclei through EFF-1 mediated fusion events during larval development (21-23).

eff-1 was initially discovered through genetic screens as the lone factor both necessary and sufficient to induce cell fusion in the *C. elegans* epidermis (22, 23). Mutations in *eff-1* lead to the disruption of embryonic fusion events in the developing hypodermal syncytium, leaving the hypodermal progenitors unfused and embryonic cell boundaries intact. *eff-1* mutant worms exhibit variable morphological and developmental defects, highlighting the importance of cell fusion for proper body morphogenesis (21, 23-25).

Here we explore the role of embryonic cell fusion in gene expression and differentiation in the developing epidermal syncytium through RNAseq of two *eff-1* mutants in which embryonic epidermal fusion is blocked. Transcriptomic analyses showed an increase in embryonic gene expression concurrent with decreased expression of larval genes. The larval genes found down-regulated in *eff-1* mutants were further found to be enriched in the epidermis and for cuticular functions. Together these findings suggest a developmental delay in the acquisition of epidermal cell fates and a possible role for cell fusion in activating gene regulatory programs associated with epidermal differentiation, adding to the growing list of functions for cell fusion and syncytialization.

Results and Discussion

eff-1–mediated cell fusion is required for proper developmental progression and morphology

To explore the effects of epidermal fusion on development and gene expression, we used two previously characterized *eff-1* mutants (*hy21*, P183L; *oj55*, S441L) (23) (**Fig. 1A**). *eff-1* mutant worms exhibit a bulging anterior region, tail spike defects at L1, and a Dpy

(dumpy) phenotype into adulthood, particularly in P183L (**Fig. 1B**). To visualize fusion defects in these mutants, we imaged apical junctions using AJM-1::GFP, confirming that *eff-1* mutant L1 larvae have a completely or largely unfused hyp7 (**Fig. 1C,D**). Quantitative analysis showed a small minority of mutant worms that appear to undergo sporadic successful fusion events despite carrying an *eff-1* mutation (**Fig. 1E**). We note that the original characterization of *eff-1* mutants reported complete lack of fusion in late embryonic stages, followed by resolution of unfused cells during larval development for both mutants at temperatures below 25°C (23). This would suggest that dissolution of the embryonic apical junctions begins in some capacity as early as L1, despite the presence of mutations in *eff-1.* The exact nature of the S441L and P183L substitutions and how they might differentially affect fusion across development requires further analysis.

We next characterized the developmental timing of these strains from hatching to first molt and reproductive adulthood. Both *eff-1* mutants showed developmental delays in the time to first molt and time to reach adulthood (**Fig. 1F**). Moreover, *eff-1* mutants were less synchronous than wild type, with P183L exhibiting a stronger phenotype than S441L. We also observed a low frequency of larval arrest in P183L, further highlighting developmental defects when *eff-1*–mediated fusion is disrupted. Overall, our findings match those from the original study (23).

The transition from embryo to larva is accompanied by widespread transcriptional rewiring as the newly hatched L1s begin locomotion and feeding, and many tissues and cell types acquire their terminal post-mitotic fate (26-29). Both P183L and S441L are nearly completely defective for hyp7 embryonic fusion, a process that coincides with this large shift in gene expression. Thus, we undertook transcriptomic analyses to explore the effects of an unfused epidermis on gene expression during this critical time point in development.

Disruption of cell fusion in embryonic development leads to widespread transcriptomic changes

Syncytialization is a critical step in the normal development of the worm epidermis, with the majority of embryonic fusion events forming the nascent hyp7 close to the end of embryonic development (14, 20). To assess the role of cell fusion and syncytialization in the embryonic-to-larval transition, we conducted RNAseq on synchronized L1 wild-type (WT) and *eff-1* mutant animals. Differential expression analysis releveled 1005 and 2608 differentially expressed genes (DEGs) with a false-discovery rate (FDR) cutoff of <0.05 in S441L and P183L, respectively (**Fig. 2A**). We observed strong overlap between the two *eff-1* mutants, with 612 shared DEGs that were differentially regulated in the same direction (422 downregulated and 190 upregulated) (**Fig. 2B**). Hierarchical clustering of top DEGs also showed high concordance between the *eff-1* mutant transcriptomes, with many shared DEGs and even more genes with fold changes in the same direction (**Fig. 2C,D**). Taken together, these data indicate a shared transcriptomic response to a lack of fusion in both *eff-1* mutants. We note that the number of DEGs and the magnitude of their fold changes were somewhat higher in the P183L mutant, corresponding to the more severe developmental defects and delays observed in this strain (**Fig. 1F**) as compared with the less penetrant S441L mutant. This raises the possibility that a slight increase in sporadic fusion of hyp7 in S441L larvae prior to the timepoint we sequenced could potentially attenuate some of the transcriptomic changes seen in the fusion-defective transcriptome. The fact that both *eff-1* mutants show significant overlap in both DEGs and overall fold changes suggests that, regardless of the individual mutation or genetic background, there is a common transcriptomic response linked to the disruption of epidermal fusion.

eff-1 mutant transcriptional changes are consistent with a developmental delay that primarily affects the epidermis

To explore the transcriptomic response to disrupted fusion, we intersected DEGs shared by both *eff-1* mutants with wild type gene expression from developmental timepoints throughout the worm lifecycle (30, 31). For the genes downregulated in *eff-1* mutants, this intersection revealed a striking enrichment of L1 associated genes (**Fig. 3A**). The converse was true of the upregulated DEGs, which showed a higher overlap with late-embryonically expressed genes. Furthermore, genes that were not differentially

expressed (FDR > 0.05) were almost all genes that are not upregulated or downregulated across development (**Fig. 3A**). This would suggest that the shift in expression from late-embryonic to L1 larval genes is prevented or delayed in worms that are *eff-1* fusion deficient.

To confirm that *eff-1* mutant L1s inappropriately maintain high embryonic gene expression and low larval gene expression, we performed a linear regression on expression data across embryonic and larval timepoints collected from modENCODE to identify gene sets that were developmentally upregulated or downregulated between late-embryonic and larval stages. We then compared average fold changes of these gene sets in our *eff-1* mutants, showing a net increase in developmentally downregulated genes and a decrease in developmentally upregulated genes for both strains (**Fig. 3B**). This reinforced the conclusion that without *eff-1* there is a delay in the acquisition of many L1-associated genes.

Although we took care to ensure synchronization at L1 of wild-type and *eff-1* mutants before mRNA collection, this does not preclude a general developmental delay and/or non-cell-autonomous effects. To begin to address direct effects of these mutations, we intersected “gold standard” lists of tissue-specific genes from small-scale single-tissue experiments with the *eff-1* DEGs (32). This analysis showed a significant enrichment for genes associated with the hyp7 syncytium, hypodermis, and epithelial system, over other non-syncytial tissues (**Fig. 3C**). This enrichment was also predominantly concentrated in the downregulated DEGs, consistent with a model in which unfused hyp7 progenitors fail to upregulate genes found in the L1 syncytial hypodermis. This would suggest that the observed transcriptomic changes are, in large part, the direct product of an unfused epidermis rather than a systemic developmental delay.

The hyp7 syncytium has many functions across larval development, including production of the cuticle through the production and secretion of apical extracellular matrix (aECM) proteins including collagen components (33-37). Gene Ontology enrichment analysis showed a substantial number of terms associated with epidermal-specific processes

including structural constituent of cuticle, collagen trimer, and collagen-containing ECM (**Fig. 3D**), adding support to the notion that normal hypodermal differentiation and function are disrupted or delayed in *eff-1* mutants. Along with the tissue enrichment analysis, these data suggest that the changes to gene expression observed in fusion-defective worms occur primarily among genes and pathways associated with the epidermis and epidermal functions over other cell and tissue types.

Nevertheless, we did observe changes in other cell types, which may be due to secondary or non-cell-autonomous effects. Interesting, the most enriched anatomical category after the epidermis was neurons and the top GO term was associated with the neurotransmitter acetylcholine. Many neurons share a close lineal history with the epidermal cells contributing to hyp7 as well as pierce the hyp7 syncytium, and the absence of cell fusion could affect their targeting and function (35, 38, 39). Later in development *eff-1* is also required for dendritic sculpting and axonal regeneration, and *eff-1* expression is observed in some neurons despite these cells never forming syncytia (40-42). As such there could be non-fusogenic functions of *eff-1* in neurons that have transcriptional consequences, although these seem to produce minimal effects as compared with the epidermal changes observed. In addition to cuticle formation, the hypodermis is essential for many metabolic and endocytic pathways involved in signaling that have non-cell-autonomous effects, perhaps explaining the enrichment of other tissue type and GO terms (**Fig. 3C,D**) (35, 43-45).

in situ **hybridization of differentially expressed transcripts in *eff-1* mutants**

To validate findings from RNAseq studies, we conducted single-molecule inexpensive fluorescence *in situ* hybridization (smiFISH) to visualize two DEGs identified in our RNAseq data, *col-42* and *rhy-1*. *col-42* encodes a structural collagen restricted to larvae and adults and was significantly downregulated in both *eff-1* mutants (**Fig. 4A**). This gene is expressed during early larval development, and smiFISH imaging showed almost no detectable signal in *eff-1* mutants at L1 (**Fig. 4A**). *rhy-1* is a transmembrane acyltransferase expressed embryonically in the epidermis (46, 47), and RNAseq detected increased *rhy-1* expression in both *eff-1* mutants (**Fig. 4B**). Consistent with this, the

number of *rhy-1* mRNA fluorescent puncta was also elevated in *eff-1* mutants (**Fig. 4B**). Collectively, our data support the central finding that fusion plays a critical role in promoting the timely differentiation and function of the epidermis based on hallmark changes in gene expression.

There has been some debate over the fate of unfused cells in the hypodermis, with one study finding unfused cells incapable of expressing the hyp7 marker *dpy-7* and speculating that there is a “hypodermalizing” signal needed for differentiation that does not cross unfused cell boundaries (25). A contradictory study found that unfused cells were largely capable of expressing *dpy-7* but noted the occasional reversion back to their progenitor fate, suggesting there are at least some fusion-dependent mechanisms that enforce differentiation (24). Both studies were conducted later in larval development and do not preclude a model in which there is an initial delay due to a lack of fusion as our study suggests. Further studies leveraging emerging single-nuclei technologies may help to uncover the precise fate of these unfused progenitors and help to uncover specification factors shared during fusion.

Materials and Methods:

Strains used and maintenance

C. elegans strains were maintained according to standard protocols and were propagated at 22°C . WH171: *eff-1*(oj55); jcIs1 *[ajm-1::GFP + unc-29(+) + rol-6(su1006)]* and BP76: *eff-1*(hy21); jcIs1 *[ajm-1::GFP + unc-29(+) + rol-6(su1006)]* were the two eff-1 mutant strains used. MH1384: *[kuIs46 (ajm-1::GFP; unc-119(+))]* was used to compare WT AJM-1::GFP to e*ff-1* mutants.

Developmental timing analysis

Time to hatch was determined by plating young adult worms, allowing them to lay eggs for 2 hours, and then removing the adults and measuring the percentage of unhatched eggs that remained over time. Time to molt was determined by plating synchronized L1 larvae and watching for cessation of pharyngeal pumping to mark the beginning of the

L1–L2 molt. Time to adulthood was measured by plating synchronized L1 larvae and noting the presence of embryos in the gonads. All experiments were carried out at 22ºC.

Microscopy

Confocal images for **Figs. 1** and **4** were taken using CellSens on an Olympus Spin-SR, Spinning Disc, Super Resolution System using an inverted Olympus IX83 microscope and Yokogawa W1 spinning disc. smiFISH images were taken of worms fixed in methanol/acetone as described (48). Larvae for **Fig. 1** images were prepared in 10 mM levamisole on 3% agarose pads.

RNA isolation and sequencing

L1s were synchronized by bleaching gravid adults and allowing embryos to arrest in M9. L1s were spun down and lysed for RNA collection via the Direct-zol kit from Zymo. RNA quality was confirmed using an Agilent Tapestation with minimum RINs of 8.0. mRNA libraries were constructed using Truseq kits from Illumina and were sequenced on Illiumina Nextseq P3 (paired-end, 100 cycles).

Transcriptomic analysis

Paired-end reads were processed using the following: low-quality reads were filtered using fastp, quality was assessed using fastQC. Reads were aligned using STAR and pseudoaligned using Salmon to the *ce11* reference genome, duplicates were removed using picard, and counts were collected using htseq (49-51). Differential expression was determined using DESeq2 (v. 1.42.1), with counts filtered for >1 TPM across all samples . DEGs were specified as those with a Benjamini-Hochberg adjusted p-value < 0.05 and $\log_2$(fold change) > 0.5 or < –0.5. Heatmaps were generated using the seaborn clustermap() function using Euclidian distance to obtain hierarchal linkages and z-score normalization by rows. Intersectional analysis was done by collecting modENCODE developmental expression data, processed in Hutter and Soh 2016 (30, 31). Upregulated, downregulated, and unchanged classifications were determined by performing a linear regression across the developmental time points data and collecting genes with a derived slope of >1 or < –1.

GO term analysis

GO term enrichment was carried out using topGO. (v. 2.54.0) on ontologies from Wormbase using the “weight01” algorithm and significance assessed with a Fisher’s statistic. Genes found to be differentially expressed (FDR < 0.05) in both S441L and P183L were used as the test set, and the background gene set was specified as genes with base mean TPM of >1 in all three transcriptomes.

Tissue enrichment

“Gold standard” tissue-specific gene sets were obtained from https://worm.princeton.edu/ (32) and compared to DEGs from the *eff-1* mutant RNAseq data, fischer’s exact test was used to calculate whether enrichment was significant.

smiFISH

smiFISH was carried out as described (48). Probe sets were designed against *col-42* and *rhy-1* using Oligostan with FLAP-X extensions (52). The FLAP-X secondary probes were labeled with Quasar 670 from Biosearch Technologies. Quantification was done in FIJI by manually drawing ROIs around embryos and L1s of appropriate age and sufficient fixation, thresholding across experimental replicates, and using the “analyze particles” option.

Acknowledgements

This work was supported by the National Institutes of Health grants GM136236 and GM125091 to D.S.F. and GM134885 to D.L.L. This project was also supported by an Institutional Development Award (IDeA) from the National Institute of General Medical Sciences of the National Institutes of Health under P20GM103432. We thank Amy Fluet for editing this manuscript. Content is solely the responsibility of the authors.

Author contributions

Conceptualization, OHF, DLL, DSF; Investigation, OHF; Writing – Original Draft, OHF; Writing – Review & Editing, OHF, DLL, DSF; Funding Acquisition, DLL, DSF; Supervision, DLL, DSF.

References

1. B. M. Ogle, M. Cascalho, J. L. Platt, Biological implications of cell fusion. *Nat Rev Mol Cell Biol* **6**, 567-575 (2005).
2. S. J. Calvert *et al.*, Studies of the dynamics of nuclear clustering in human syncytiotrophoblast. *Reproduction* **151**, 657-671 (2016).
3. P. J. Brooks, M. Glogauer, C. A. McCulloch, An Overview of the Derivation and Function of Multinucleated Giant Cells and Their Role in Pathologic Processes. *Am J Pathol* **189**, 1145-1158 (2019).
4. L. I. Larsson, B. Bjerregaard, J. F. Talts, Cell fusions in mammals. *Histochem Cell Biol* **129**, 551-561 (2008).
5. S. M. Abmayr, G. K. Pavlath, Myoblast fusion: lessons from flies and mice. *Development* **139**, 641-656 (2012).
6. M. Roper, C. Ellison, J. W. Taylor, N. L. Glass, Nuclear and genome dynamics in multinucleate ascomycete fungi. *Curr Biol* **21**, R786-793 (2011).
7. J. J. Dowling, C. C. Weihl, M. J. Spencer, Molecular and cellular basis of genetically inherited skeletal muscle disorders. *Nat Rev Mol Cell Biol* **22**, 713-732 (2021).
8. M. Cardamone, B. T. Darras, M. M. Ryan, Inherited myopathies and muscular dystrophies. *Semin Neurol* **28**, 250-259 (2008).
9. Y. Iosilevskii, B. Podbilewicz, Programmed cell fusion in development and homeostasis. *Curr Top Dev Biol* **144**, 215-244 (2021).
10. T. L. Orr-Weaver, When bigger is better: the role of polyploidy in organogenesis. *Trends Genet* **31**, 307-315 (2015).
11. O. Deshpande, J. de-Carvalho, D. V. Vieira, I. A. Telley, Astral microtubule cross-linking safeguards uniform nuclear distribution in the Drosophila syncytium. *J Cell Biol* **221** (2022).
12. S. Demin, M. Berdieva, A. Goodkov, Cell-cell fusions and cell-in-cell phenomena in healthy cells and cancer: Lessons from protists and invertebrates. *Semin Cancer Biol* **81**, 96-105 (2022).
13. E. H. Chen, E. Grote, W. Mohler, A. Vignery, Cell-cell fusion. *FEBS Lett* **581**, 2181-2193 (2007).
14. S. Alper, B. Podbilewicz, Cell fusion in Caenorhabditis elegans. *Methods Mol Biol* **475**, 53-74 (2008).
15. P. S. Aguilar *et al.*, Genetic basis of cell-cell fusion mechanisms. *Trends Genet* **29**, 427-437 (2013).
16. M. Kim *et al.*, Single-nucleus transcriptomics reveals functional compartmentalization in syncytial skeletal muscle cells. *Nat Commun* **11**, 6375 (2020).
17. M. J. Petrany *et al.*, Single-nucleus RNA-seq identifies transcriptional heterogeneity in multinucleated skeletal myofibers. *Nat Commun* **11**, 6374 (2020).
18. K. Williams, K. Yokomori, A. Mortazavi, Heterogeneous Skeletal Muscle Cell and Nucleus Populations Identified by Single-Cell and Single-Nucleus Resolution Transcriptome Assays. *Front Genet* **13**, 835099 (2022).

19. X. Liu *et al.*, Analysis of cell fate from single-cell gene expression profiles in C. elegans. *Cell* **139**, 623-633 (2009).
20. B. Podbilewicz, J. G. White, Cell fusions in the developing epithelial of C. elegans. *Dev Biol* **161**, 408-424 (1994).
21. B. Podbilewicz *et al.*, The C. elegans developmental fusogen EFF-1 mediates homotypic fusion in heterologous cells and in vivo. *Dev Cell* **11**, 471-481 (2006).
22. G. Shemer *et al.*, EFF-1 is sufficient to initiate and execute tissue-specific cell fusion in C. elegans. *Curr Biol* **14**, 1587-1591 (2004).
23. W. A. Mohler *et al.*, The type I membrane protein EFF-1 is essential for developmental cell fusion. *Dev Cell* **2**, 355-362 (2002).
24. S. L. Koneru *et al.*, A role for the fusogen eff-1 in epidermal stem cell number robustness in Caenorhabditis elegans. *Sci Rep* **11**, 9787 (2021).
25. C. Brabin, P. J. Appleford, A. Woollard, The Caenorhabditis elegans GATA factor ELT-1 works through the cell proliferation regulator BRO-1 and the Fusogen EFF-1 to maintain the seam stem-like fate. *PLoS Genet* **7**, e1002200 (2011).
26. J. I. Murray *et al.*, Automated analysis of embryonic gene expression with cellular resolution in C. elegans. *Nat Methods* **5**, 703-709 (2008).
27. M. E. Boeck *et al.*, The time-resolved transcriptome of C. elegans. *Genome Res* **26**, 1441-1450 (2016).
28. J. Cao *et al.*, Comprehensive single-cell transcriptional profiling of a multicellular organism. *Science* **357**, 661-667 (2017).
29. J. S. Packer *et al.*, A lineage-resolved molecular atlas of. *Science* **365** (2019).
30. M. B. Gerstein *et al.*, Integrative analysis of the Caenorhabditis elegans genome by the modENCODE project. *Science* **330**, 1775-1787 (2010).
31. H. Hutter, J. Suh, GExplore 1.4: An expanded web interface for queries on. *Worm* **5**, e1234659 (2016).
32. R. Kaletsky *et al.*, Transcriptome analysis of adult Caenorhabditis elegans cells reveals tissue-specific gene and isoform expression. *PLoS Genet* **14**, e1007559 (2018).
33. G. J. Hendriks, D. Gaidatzis, F. Aeschimann, H. Großhans, Extensive oscillatory gene expression during C. elegans larval development. *Mol Cell* **53**, 380-392 (2014).
34. M. W. Meeuse *et al.*, Developmental function and state transitions of a gene expression oscillator in Caenorhabditis elegans. *Mol Syst Biol* **16**, e9498 (2020).
35. A. D. Chisholm, T. I. Hsiao, The Caenorhabditis elegans epidermis as a model skin. I: development, patterning, and growth. *Wiley Interdiscip Rev Dev Biol* **1**, 861-878 (2012).
36. I. L. Johnstone, Cuticle collagen genes. Expression in Caenorhabditis elegans. *Trends Genet* **16**, 21-27 (2000).
37. A. P. Page, I. L. Johnstone, The cuticle. *WormBook*, 1-15 (2007).
38. J. E. Sulston, E. Schierenberg, J. G. White, J. N. Thomson, The embryonic cell lineage of the nematode Caenorhabditis elegans. *Dev Biol* **100**, 64-119 (1983).
39. A. Bounoutas, M. Chalfie, Touch sensitivity in Caenorhabditis elegans. *Pflugers Arch* **454**, 691-702 (2007).

40. M. Oren-Suissa, T. Gattegno, V. Kravtsov, B. Podbilewicz, Extrinsic Repair of Injured Dendrites as a Paradigm for Regeneration by Fusion in. *Genetics* **206**, 215-230 (2017).
41. M. Oren-Suissa, D. H. Hall, M. Treinin, G. Shemer, B. Podbilewicz, The fusogen EFF-1 controls sculpting of mechanosensory dendrites. *Science* **328**, 1285-1288 (2010).
42. T. Zhu, X. Liang, X. M. Wang, K. Shen, Dynein and EFF-1 control dendrite morphology by regulating the localization pattern of SAX-7 in epidermal cells. *J Cell Sci* **130**, 4063-4071 (2017).
43. M. Fukuyama, K. Kontani, T. Katada, A. E. Rougvie, The C. elegans Hypodermis Couples Progenitor Cell Quiescence to the Dietary State. *Curr Biol* **25**, 1241-1248 (2015).
44. D. Katsanos *et al.*, Gene expression profiling of epidermal cell types in C. elegans using Targeted DamID. *Development* **148** (2021).
45. R. H. Dowen, P. C. Breen, T. Tullius, A. L. Conery, G. Ruvkun, A microRNA program in the C. elegans hypodermis couples to intestinal mTORC2/PQM-1 signaling to modulate fat transport. *Genes Dev* **30**, 1515-1528 (2016).
46. C. Shen, Z. Shao, J. A. Powell-Coffman, The Caenorhabditis elegans rhy-1 gene inhibits HIF-1 hypoxia-inducible factor activity in a negative feedback loop that does not include vhl-1. *Genetics* **174**, 1205-1214 (2006).
47. D. K. Ma, R. Vozdek, N. Bhatla, H. R. Horvitz, CYSL-1 interacts with the O2-sensing hydroxylase EGL-9 to promote H2S-modulated hypoxia-induced behavioral plasticity in C. elegans. *Neuron* **73**, 925-940 (2012).
48. D. M. Parker, L. P. Winkenbach, A. Parker, S. Boyson, E. O. Nishimura, Improved Methods for Single-Molecule Fluorescence In Situ Hybridization and Immunofluorescence in Caenorhabditis elegans Embryos. *Curr Protoc* **1**, e299 (2021).
49. A. Dobin *et al.*, STAR: ultrafast universal RNA-seq aligner. *Bioinformatics* **29**, 15-21 (2013).
50. R. Patro, G. Duggal, M. I. Love, R. A. Irizarry, C. Kingsford, Salmon provides fast and bias-aware quantification of transcript expression. *Nat Methods* **14**, 417-419 (2017).
51. S. Anders, P. T. Pyl, W. Huber, HTSeq--a Python framework to work with high-throughput sequencing data. *Bioinformatics* **31**, 166-169 (2015).
52. N. Tsanov *et al.*, smiFISH and FISH-quant - a flexible single RNA detection approach with super-resolution capability. *Nucleic Acids Res* **44**, e165 (2016).

Figure Legends:

Figure 1. *eff-1* mutant worms display morphological defects and developmental delay. A) Diagram of the *eff-1* locus, with mutant alleles P183L (*hy21*) and S441L (*oj55*) indicated. Dark blue marks the predicted extracellular domain, pink the transmembrane domain, and gold the cytoplasmic domain. B) Brightfield imaging of wild-type (WT) and *eff-1* mutant L1 and adult animals. Scale bars are 10 μm for L1s and 100 μm for adults. C) Schematic of the L1 hypodermis, with *eff-1*–mediated fusion events marked with dashed green lines. Ventral precursor cells are in red. D) Representative images of AJM-1::GFP fluorescence in WT and *eff-1* mutant L1 larvae marking apical junctions of seam cells (both genotypes) and unfused hypodermal progenitor cells (*eff-1* mutants). E) Quantification of the fraction of L1 worms with at least one fusion event (fisher's exact test, p = 0.337, n of at least 50 per genotype). F) Quantification of developmental timepoints in WT and *eff-1* mutants. Time to hatch was measured via observation for hatched eggs and locomotion. Time to first molt was measured via the cessation of pharyngeal pumping. Time to adulthood from L1 was measured by sexual maturity. N of at least 50 individuals per strain**,** per developmental timepoint.

Figure 2. RNAseq of two *eff-1* mutants show a common transcriptomic response to the disruption of epidermal fusion. A) Volcano plot of top DEGs (downregulated in blue and upregulated in red) for *eff-1* mutants *hy21* and *oj55.* B) Experimental overlap of DEGs between *eff-1* (*hy21*) and (*oj55*). Hypergeometric distribution significance values of $3.31356e^{-161}$ for downregulated genes and 0.00309 for upregulated genes. C) Aligned heatmap of top DEGs in *eff-1* mutants. Colors correspond to z-score–normalized fold change. D) MA (log normalized expression vs fold change) plots of each *eff-1* mutant, with upregulated and downregulated DEGs from the other mutant colored red and blue, respectively. DEGs upregulated and downregulated in the P183L mutant are more often differentially expressed in the same direction in S441L. This is also true for S441L DEGs with respect to P183L fold changes. Righthand profile plots of kernel density estimates for upregulated and downregulated gene distributions of the corresponding genotype.

Figure 3. Transcriptomic changes in *eff-1* mutants correspond to a developmental delay in the hypodermis. A) Normal developmental trajectories of genes in wild type (WT) that are upregulated (red), downregulated (blue), or developmentally constant (gray) in *eff-1* mutants at L1. Fusion-defective transcriptomes show a marked increase in embryonic transcripts with a concurrent loss of larval transcripts. Dashed line indicates an approximate hatching time of 800 min. Shaded regions represent a confidence interval of 95%. Diagrams below illustrate general trends of the three groups of genes and the proposed effect of fusion disruption on their developmental trajectory. B) Average $\log_2$(fold change) of all genes categorized as developmentally downregulated (left) or upregulated (right) in WT data for *eff-1* P183L (green) and S441L (purple) at L1. Categorization was based on linear regression across developmental time from WT expression datasets; error bars represent standard error (31). C) Tissue enrichment analysis of DEGs based on "gold standard" small-scale enrichment experiments (32). DEGs were intersected with tissue-specific gene lists, and p-values were calculated based on hypergeometric significance. D) GO-term analysis of overlapping DEGs using topGO and WormBase gene ontology terms. "Sig. / Exp." Indicates the number of significantly differentially expressed genes shared between the *eff-1* mutants found per GO term vs. the expected number. p-value's calculated using fisher's exact test.

Figure 4. smiFISH of DEGs in *eff-1* fusion mutants.

A) Representative images of *col-42* smiFISH hybridization in L1s. mRNA were quantified based on the number of fluorescent puncta. RNAseq counts (transcripts per million, TPM) for *col-42* mRNA in WT and *eff-1* mutants. Normal developmental trajectory of *col-42* expression taken from modENCODE expression data. B) Representative images of *rhy-1* smiFISH hybridization in late-stage embryos, with experimentally derived RNAseq counts and longitudinal expression data as in A.

Figure 1

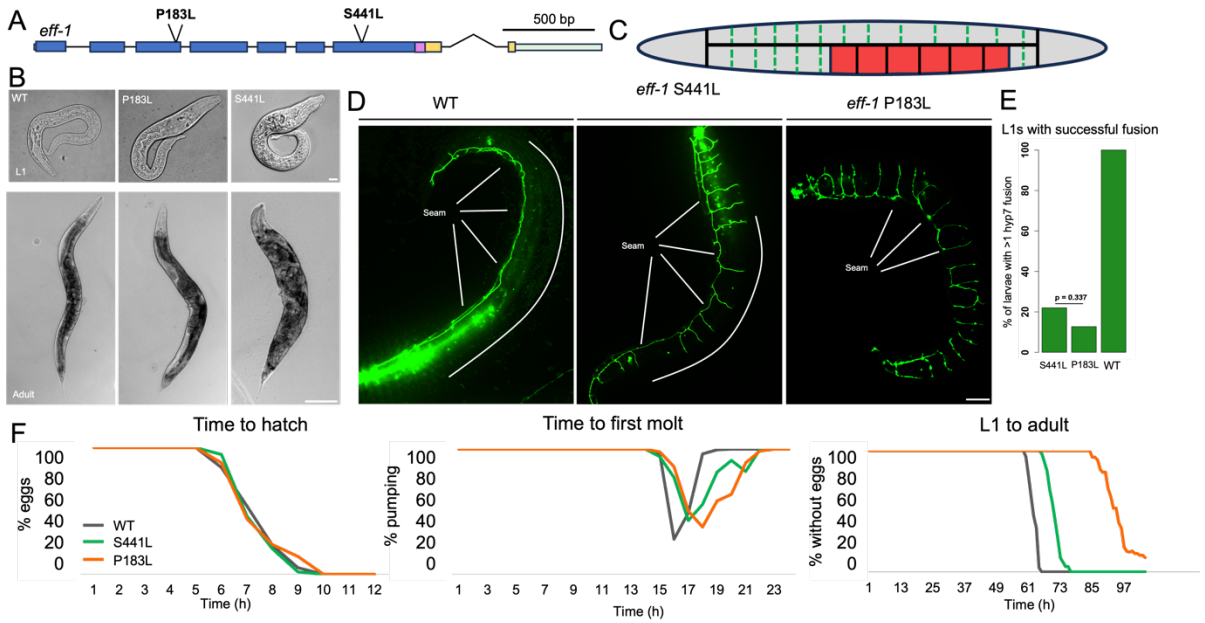

Figure 2

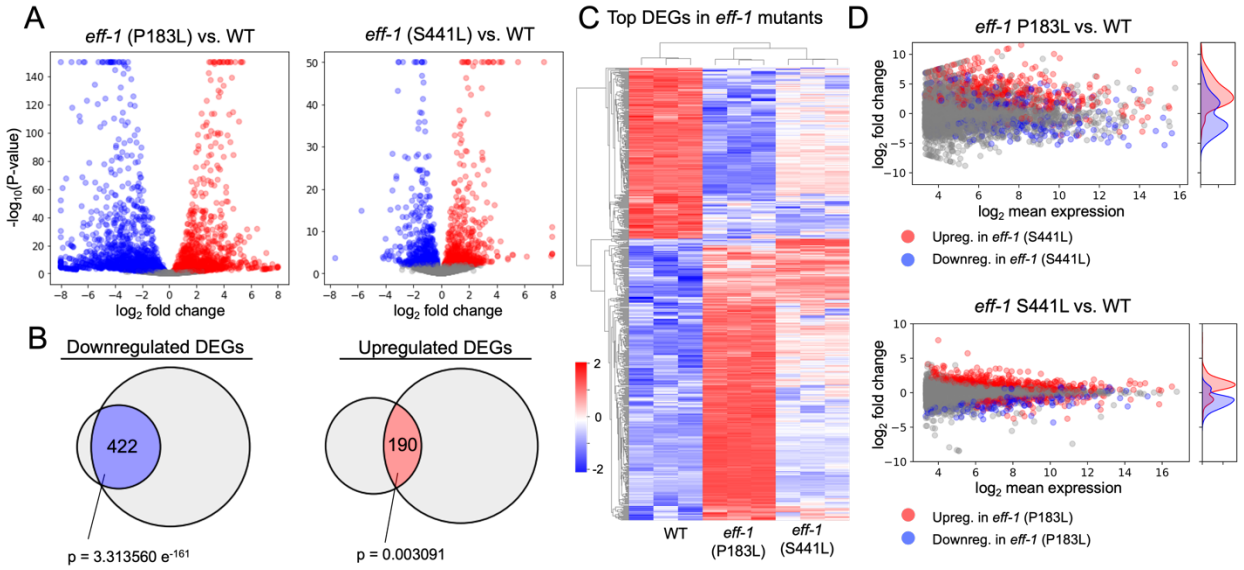

Figure 3

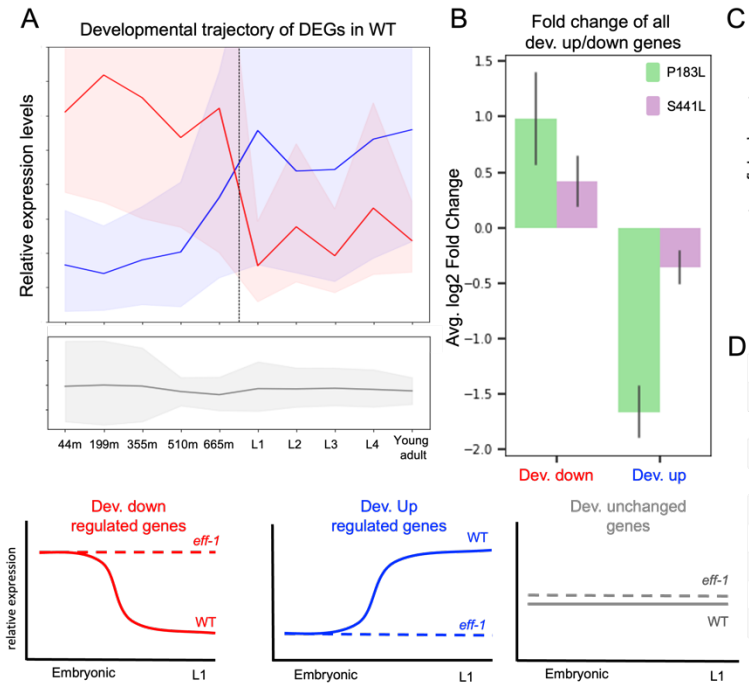

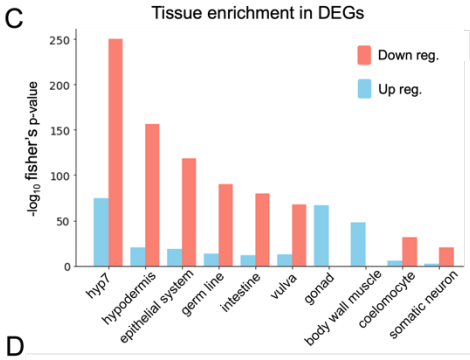

D

GO Term	Sig./Exp.	p-Value
Acetylcholine transport	6/1	0.00017
Structural constituent of cuticle	17/7	0.00025
Collagen trimer	16/6	0.00051
Monoatomic ion transmembrane transport	34/20	0.00314
Anatomical structure development	93/77	0.00605
Nuclear pore	6/2	0.00719
Collagen-containing ECM	8/3	0.01036
miRNA processing	4/1	0.01085
Regulation of cell cycle process	16/9	0.01059
Zinc ion binding	29/19	0.01179
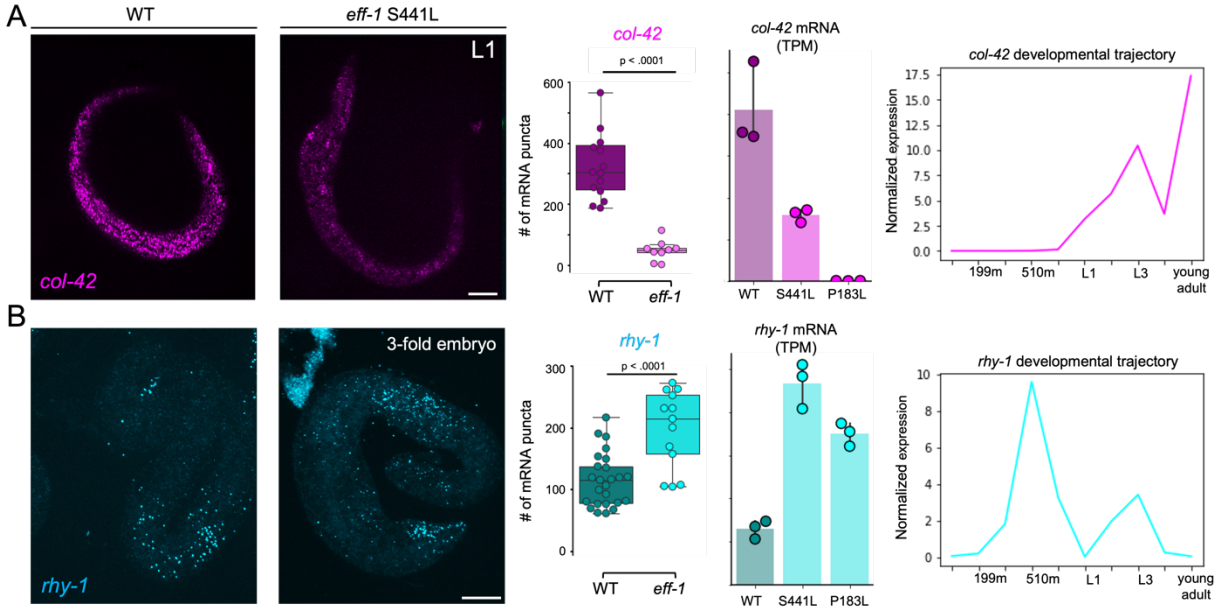
Figure 4